Journal Name

RSCPublishing

ARTICLE

Nanoscale Self-Assembled Multivalent (SAMul) Heparin Binders in Highly Competitive, Biologically Relevant, Aqueous Media

Cite this: DOI: 10.1039/x0xx00000x

Received 00th January 2012,
Accepted 00th January 2012

DOI: 10.1039/x0xx00000x

www.rsc.org/

Stephen M. Bromfield,[a,‡] Paola Posocco,[b,c,‡] Ching Wan Chan,[a] Marcelo Calderon,[d] Scott R. Guimond,[e] Jeremy E. Turnbull,[e] Sabrina Pricl,[b,c,*] and David K. Smith*[a]

This paper investigates small molecules that self-assemble to display multivalent ligand arrays for heparin binding. In water, the self-assembled multivalent (SAMul) heparin binder is highly competitive with the current clinical heparin reversal agent, protamine. On addition of salt, the dimensions of the self-assembled nanostructure increase. This unique feature is due to the dynamic, responsive nature of assembly, predicted using multiscale modelling and proven experimentally, enhancing heparin binding of SAMul systems relative to fixed covalent multivalent nanostructures. Conversely, the presence of serum adversely affects the heparin binding of SAMul systems relative to covalent nanostructures due to partial destabilisation of the assemblies. Nonetheless, clotting assays in human plasma demonstrate that the SAMul system acts as a functional heparin reversal agent. Compound degradation, inducing nanostructure disassembly and loss of SAMul binding, takes place over 24 hours due to ester hydrolysis – but when bound to heparin, stability is enhanced. Heparin reversal in plasma, and the therapeutically useful degradation profile, make this SAMul approach of potential therapeutic value in replacing protamine, which has a number of adverse effects when used in the clinic.

Introduction

There is intense activity in the emerging field of nanomedicine.[1] Biomolecules and biological structures have nanoscale dimensions, and designing synthetic systems which can interact with biological targets on the nanoscale is therefore an area of key interest.[2] Multivalency is an effective and widely employed way of achieving high-affinity interactions between nanoscale surfaces.[3] However, covalent multivalent systems often involve complex multi-step syntheses, and may persist in vivo long after they have had their desired effect. One approach to making multivalent systems which are synthetically simpler and more responsive is to design low-molecular-weight drug-like ligands, which spontaneously self-assemble into a nanoscale ligand array – Self Assembled Multivalency (SAMul).[4] This approach has been used to organise a range of ligands, including saccharides and peptides, and enhance their binding to nanoscale biological surfaces.[5]

A particularly interesting nanoscale target for binding is heparin (Fig. 1).[6] This anionic polysaccharide plays key roles in the coagulation cascade, and is in widespread clinical use as an anti-coagulant during surgery.[7] In the clinic, after surgery, the effect of heparin must be reversed so clotting can begin. This is typically achieved using protamine (Fig. 1), a cationic arginine-rich protein which binds heparin electrostatically.[8] Unfortunately, protamine causes adverse effects in a significant number of patients,[9] which limits its ability to be applied at high doses. This can lead to problems with heparin rebound.[10]

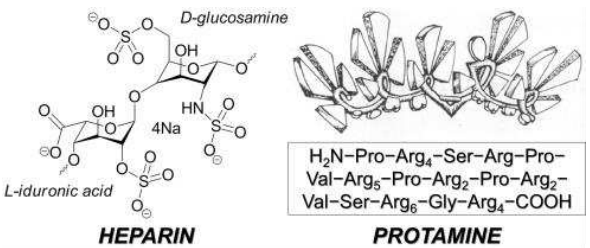

Figure 1. Major heparin disaccharide repeat unit (left) and a typical protamine (right, box).

A number of approaches have been taken to develop heparin binders as possible synthetic protamine replacements.[6] Most of these make use of cationic compounds which bind heparin electrostatically.[11] To achieve high affinity binding, multivalent cationic polymers and dendrimers have been used.[12] In general, however, such systems are either well-defined but expensive, or lower-cost but poorly-defined. Furthermore, cationic polymers often have poor toxicity profiles.[13] The

limitations of previous approaches to protamine replacement therapy encouraged us to explore an innovative self-assembly approach to multivalent heparin binding. Self-assembly can rapidly yield nanoscale multivalent surfaces for heparin binding – these structures should be more responsive than traditional covalent systems. We recently reported that ligand **C22-G1** (Fig. 2) assembled into micellar nanostructures with a critical micelle concentration (CMC) of 4 μM in phosphate buffered saline at pH 7.5, and bound heparin.[14] However, these studies were only performed in pure water – we wanted to understand these nanostructures in more challenging and bio-relevant conditions, and the influence of this on SAMul binding. This new paper reports the results, clearly demonstrates the unique advantages and limitations of a SAMul approach, and reports functional heparin reversal in human plasma.

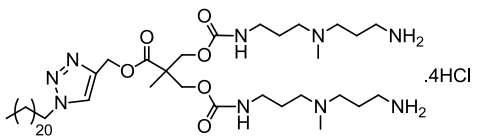

C22-G1

Figure 2. Heparin binder **C22-G1**.

Results and Discussion

Effect of Biological Salt Levels on SAMul Heparin Binding

The assay we previously employed to monitor solution-phase heparin binding with **C22-G1** used methylene blue (MB, Fig. 3) as a competitive dye, and only worked at very low ionic strengths (≤5 mM NaCl) and buffer concentrations (1 mM Tris HCl).[14] In the absence of salt, **C22-G1** required 86% as much charge as protamine to displace half of the MB from its complex with heparin. We reasoned that our recent report of the new Mallard Blue (MalB) dye,[15] would allow us to develop an assay for much more highly competitive conditions. Indeed, we recently exemplified a new competition assay using MalB, in which PAMAM dendrimers displaced the dye from its heparin complex and the UV-Vis spectroscopic response quantified their relative binding abilities.[16] We therefore performed this competition assay at biologically relevant salt and buffer conditions (150 mM NaCl and 10 mM Tris HCl).

Data are reported in terms of the effective concentration required to displace half of the MalB (EC_{50}) from heparin, the charge excess of cationic binder at this point (CE_{50}, i.e., the cation/anion ratio, assuming that **C22-G1** is tetra-cationic, and the disaccharide repeat unit of heparin is tetra-anionic with an average M_r of 665.4) and the effective dose of the binder (given in mg per 100 international units [IU] of heparin). As supplied, heparin only contains ~30-40% of chains with the sequence of pentasaccharide repeat units conferring high anti-coagulant activity. However, all of the material contains anionic saccharides, even if not active, which will be bound by cationic systems. The heparin concentration in the assay (27 μM, assuming average M_r of 665.4) refers to the total concentration of anionic disaccharide, irrespective of whether it is in the active form or not, and this value is used to calculate the CE_{50}, value. However, for calculating the 'dose' we reference the activity of the heparin binder only to the clinically active portion of heparin (as given in international units).

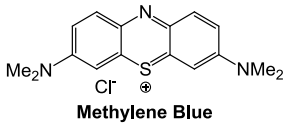

Methylene Blue

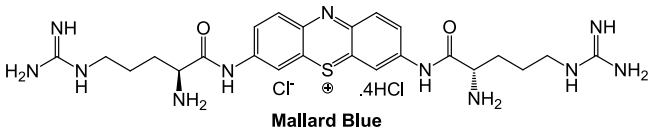

Mallard Blue

Figure 3. Methylene Blue (MB) and Mallard Blue (MalB) dyes used in competition assays to monitor heparin binding.

Table 1. Heparin Binding Data from MalB Competition Assays using 25 μM MalB and 27 μM heparin in 10 mM Tris-HCl and 150 mM NaCl.

Binder	EC_{50} (μM)	CE_{50}	Dose (mg/100IU)
C22-G1	7.50 ± 1.22	0.28 ± 0.05	0.23 ± 0.04
Protamine	2.34 ± 0.23	0.52 ± 0.05	0.32 ± 0.03
G2-PAMAM	2.55 ± 0.32	0.38 ± 0.04	0.25 ± 0.03
G4-PAMAM	0.64 ± 0.04	0.38 ± 0.02	0.27 ± 0.02

Table 1 indicates that under these highly competitive conditions, protamine and **C22-G1** bind effectively to heparin and readily displace MalB. The concentration of **C22-G1** required to displace half of MalB (EC_{50}) is significantly greater than that of protamine (or the PAMAM dendrimers), but this simply reflects the fact that **C22-G1** is a low-molecular-weight drug-like system with only 4 positive charges, while protamine has 24. Interestingly, the EC_{50} value of 7.5 μM is above the critical aggregation concentration of 4 μM calculated by Nile Red Assay[17] – indicative that self-assembly is required for effective multivalent binding.

A fairer comparison between heparin binders is provided by their charge efficiencies (CE_{50}). Here, **C22-G1** significantly outperforms protamine (indeed **C22-G1** only requires ca. 54% as much charge as protamine to displace MalB). This MalB assay therefore suggests that in high, biologically relevant amounts of salt, **C22-G1** significantly improves its heparin binding performance relative to protamine – in the absence of salt, **C22-G1** needed 86% as much charge as protamine. Furthermore, **C22-G1** was active in this assay at a very low dose (better than any of the covalent nanostructures).

It is worth noting that 7.5 μM **C22-G1** displaces half the MalB from heparin ([MalB] = 25 μM). As such, **C22-G1** is a significantly better heparin binder than MalB, which is itself already highly optimised for heparin binding in terms of shape and charge organisation.[15] This strongly suggests that self-assembly is indeed assisting multivalent binding of **C22-G1**. Interestingly, **C22-G1** even outperforms the best PAMAM dendrimers on a per charge and dose basis, in spite of the fact that G2-PAMAM has 16 positive surface charges and G4-PAMAM has 64. This clearly indicates **C22-G1** is using more than just four charges on an individual molecule to bind

heparin, and that self-assembly is marshalling positive charges to achieve high affinity binding – self-assembled multivalency (SAMul). In the absence of hydrophobic modification, such compounds are incapable of binding heparin – in agreement with our previous observations of SAMul DNA binding.[18]

Further evidence that self-assembly plays an important role in heparin binding is provided by scanning electron microscopy (SEM). As previously reported,[14] on drying mixtures of **C22-G1** and heparin, nanoscale micelles were observed clustered on the heparin surface (Fig. 4), clearly demonstrating that the nanostructures remain intact and do not appear to significantly disassemble or rearrange in the presence of heparin.

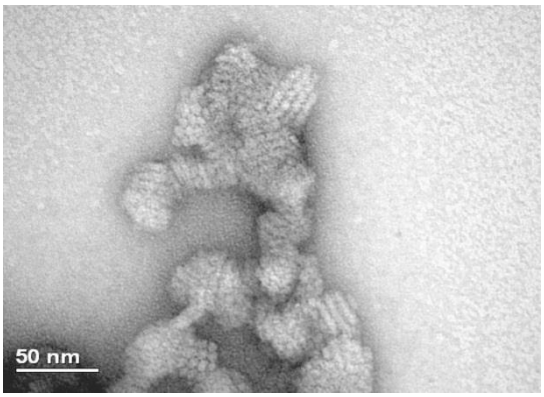

Figure 4. Scanning electron microscopy (SEM) image of **C22-G1** nanostructures in the presence of heparin, dried from aqueous solution. Reproduced with kind permission from Wiley-VCH.[14]

In our new work, this observation was also supported in the solution phase by carrying out the Nile Red assay on **C22-G1** in the presence of heparin. Nile Red was still solubilised, demonstrating that self-assemblies with a hydrophobic domain were still being formed in the presence of heparin. The critical aggregation concentration (CAC) increased slightly to 14 μM, which may suggest some destabilisation, but clearly **C22-G1** is still able to self-assemble in the presence of heparin.

The comparison of **C22-G1** with protamine and PAMAM dendrimers suggests that the flexible, responsive nature of the self-assembled array may allow **C22-G1** to better interact with heparin than the covalently fixed polycations. To probe this further, and to discover why salt improves the relative heparin binding ability of **C22-G1**, we turned to multiscale molecular modelling.[19] Using a combination of molecular dynamics (MD) and mesoscale modelling (dissipative particle dynamics, DPD), we gained unique insight into the self-assembly of this type of object in different media across multiple length scales. In this multiscale approach, we initially refine the structure of **C22-G1** by MD methods. We then parameterise and coarse-grain the structure, which allows us to use DPD methods to refine the structure of self-assemblies of multiple **C22-G1** molecules. We then overlay MD information onto the coarse-grained mesoscale assemblies and gain further detailed information into the energetics of assembly and binding. All of this modelling is performed in an appropriate solvent medium.

The simulations suggested that the addition of salt significantly changed the dimensions of the self-assembled nanostructures formed by **C22-G1**, which become much larger in 150 mM NaCl (Fig. 5). It is known that micellar aggregates can enlarge in response to increasing ionic strength,[20] an effect normally explained in terms of salt-mediated screening of micellar surface charge and an increasing contribution of the hydrophobic effect. These effects allow a larger number of individual surfactant molecules to be incorporated into the self-assembled nanostructures, hence enlarging them.

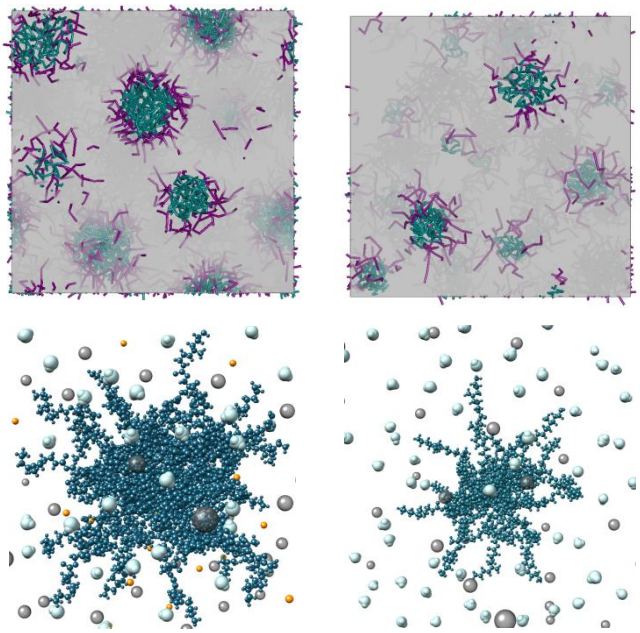

Figure 5. Mesoscale (top panel) and atomistic (bottom panel) models of self-assembled **C22-G1** under 150 mM NaCl (left) and no salt (right) conditions. In the upper panel, the hydrophobic portion of the **C22-G1** molecules is shown as teal sticks while the hydrophilic corona is portrayed in plum. The solvent and ions molecules are visualized as a continuum grey field. In the lower panel, the **C22-G1** molecules appear as steel blue sticks-and-balls. Some representative water molecules, Na^+ and Cl^- ions are also shown as light blue, orange, and grey CPK spheres, respectively.

Specifically, our simulations predict that at physiological ionic strength, **C22-G1** self-assembles into well-defined spherical micelles with an aggregation number (N_{agg}) of 24 ± 1, a total charge (Q_{tot}) of 96 ± 4, and an average micellar diameter (D_m) of 9.3 ± 0.1 nm. The absence of salt again results in the formation of spherical assemblies; but with a much smaller N_{agg} (11 ± 3) and Q_{tot} (44 ± 12) and, consequently, smaller dimensions (D_m = 6.3 ± 0.5). This change in dimensions results from a combination of charge screening and increased hydrophobic effect which, in turn, reflect in a variation of the corresponding values of the mesoscale interaction parameters (see Table S1). This result suggests that the non-covalent nature of the SAMul nanostructure allows it to respond to the environment in which it finds itself, and hence modify its size. Clearly a covalently bound nanostructure would be unable to do this to the same extent.

To confirm the predicted change in dimensions experimentally, we carried out dynamic light scattering (DLS) in the absence and presence of salt (Table 2). In the presence of 150 mM NaCl, the self-assembled nanostructure is indeed

significantly larger than in the absence of electrolyte. As such, the experimental study is fully supportive of the proposals forthcoming from multiscale modelling.

Table 2. Micellar aggregate diameter of C_{22}-G1 in the absence and presence of 150 mM NaCl as measured by DLS.

Media	Diameter (nm)	Peak Width (nm)
10 mM Tris HCl	5.8 ± 0.5	2.0
10 mM Tris HCl, 150 mM NaCl	9.1 ± 0.1	2.1

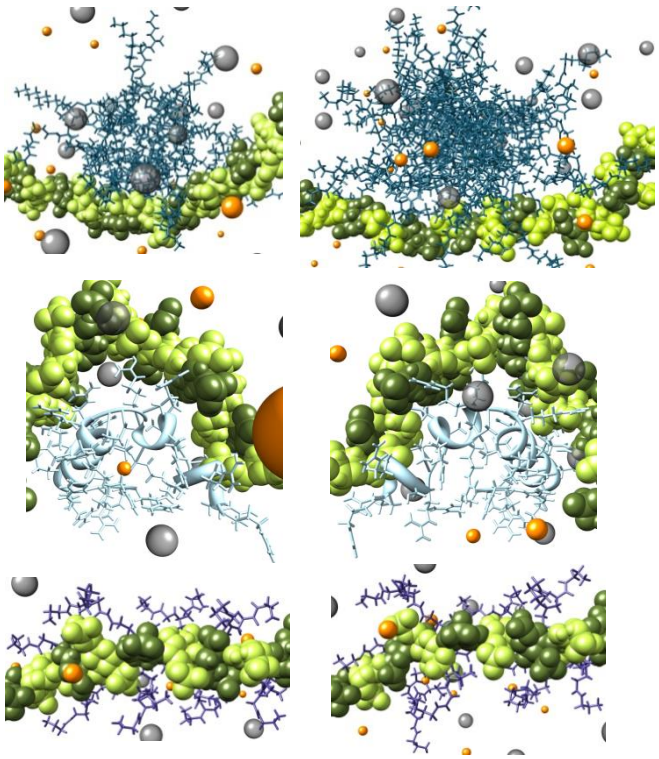

Figure 6. Atomistic models of self-assembled **C22-G1** (top panel), Protamine (middle panel), and G2-PAMAM (bottom panel) under no salt (left) and 150 mM NaCl (right) conditions. **C22-G1** is shown as teal sticks, protamine as a light blue ribbon with residues highlighted as sticks, and G2-PAMAM as dark slate sticks. Heparin is in dark olive green (L-iduronic acid) and light green (D-glucosamine) spheres. Water molecules are omitted for clarity while some Na^+ and Cl^- ions are shown as orange and grey spheres, respectively.

Given the diameter of the SAMul nanostructures increases on the addition of salt, we reasoned this may provide a mechanism through which these self-assembled structures improve their heparin binding relative to protamine as ionic strength increases. We used multiscale modelling to compare the thermodynamics of interaction of the different micellar structures, protamine and G2-PAMAM with heparin (Table 3, Fig. 6).

In the presence of salt, **C22-G1** binds heparin more effectively ($\Delta G^{eff}_{bind} = -65.0$ kcal/mol) than in its absence ($\Delta G^{eff}_{bind} = -30.2$ kcal/mol). This is primarily a result of the higher surface charge of the larger micelle formed in the presence of salt. However, we can also determine how effectively each individual charge binds to heparin. In the absence of salt, the micelles formed by **C22-G1** have a total charge of only +44, 18 of which (Q_{eff}) are effectively engaged in binding heparin (Fig. 6, top left), resulting in $\Delta G^{eff}_{bind}/Q_{eff}$ of -1.68 kcal/mol (Table 3). On the other hand, in 150 mM NaCl, the larger self-assembled micelles generated by **C22-G1** exploit 32 (out of 96) positive charges to constantly bind heparin (see Fig. 6, top right) in a more efficient manner, as testified by the more favourable $\Delta G^{eff}_{bind}/Q_{eff}$ value of -2.03 kcal/mol (Table 3). The larger more flexible micelle is therefore not only a stronger binder overall, but each individual charge has more effective binding – for a full deconvolution of the origins of these enhanced binding effects – see below.

Table 3. Predicted number of effective charges (Q_{eff}), effective free energy of binding (ΔG^{eff}_{bind}), and effective-charge-normalized free energy of binding ($\Delta G^{eff}_{bind}/Q_{eff}$) for C22-G1, Protamine and G2-PAMAM binding heparin under high salt/no salt conditions.

Binder	Q_{eff}	ΔG^{eff}_{bind} (kcal/mol)	$\Delta G^{eff}_{bind}/Q_{eff}$ (kcal/mol)
150 mM NaCl			
C22-G1	32 ± 1	-65.0 ± 1.6	-2.03± 0.08
Protamine	12 ± 1	-3.96 ± 0.41	-0.33 ± 0.04
G2-PAMAM	13 ± 1	-16.9 ± 0.5	-1.30 ± 0.11
0 NaCl			
C22-G1	18 ± 2	-30.2 ± 1.0	-1.68± 0.19
Protamine	10 ± 1	-2.60 ± 0.30	-0.26± 0.04
G2-PAMAM	15 ± 1	-22.1 ± 0.8	-1.47± 0.03

According to our calculations, protamine (modelled on a typical protamine sequence, as previously reported)[16] is only marginally improved by the presence of salt ($\Delta G^{eff}_{bind}/Q_{eff}$ (150 mMNaCl) - $\Delta G^{eff}_{bind}/Q_{eff}$ (no salt) = -0.07 kcal/mol). This can be ascribed to a balanced contribution of counteracting factors including the rigid tertiary structure of protamine being less affected by a high-salt environment, the greater screening of electrostatic interactions, and greater compaction of the polysaccharide polyelectrolyte which may increase intermolecular contacts (Fig. 6, middle panel). Ionic strength appears to play a detrimental role in the formation of G2-PAMAM/heparin complex (ΔG^{eff}_{bind}), an effect we propose is due to the external ions weakening the electrostatic interactions which form the relevant complex. We suggest that coupled to the limited structural reorganization of the covalently bound nanostructure, G2-PAMAM becomes a less effective heparin binder at physiological ionic strength (Fig. 6, lower panel).

To further support our hypothesis and investigate in detail the nature of the intermolecular interactions steering the binding process we deconvoluted the enthalpic term of the effective free energy of binding ΔG^{eff}_{bind} into its different components. From this analysis we found that, for both G2-PAMAM and **C22-G1**, and independently of the salt conditions applied, heparin binding is, as expected substantially driven by the total electrostatic term. In all cases the desolvation free energy penalty paid by the systems upon complexation (ΔG^{eff}_{GB}) is more than compensated by the favourable electrostatic interactions between heparin and its binders (ΔE^{eff}_{ele}), so that the total electrostatic term ($\Delta E^{eff}_{ele,tot} = \Delta E^{eff}_{ele} + \Delta G^{eff}_{GB}$, Table S2) always contributes favourably to the binding. For G2-PAMAM the value of $\Delta E^{eff}_{ele,tot}$ is -20.11 kcal/mol in the absence of salt

and -16.07 kcal/mol at 150 mM NaCl – i.e. the presence of salt diminishes the electrostatic term. The same total electrostatic component of ΔG^{eff}_{bind} for **C22-G1** is equal to -33.49 kcal/mol and -67.97 kcal/mol under no/high salt conditions, respectively – even taking into account the larger number of **C22-G1** molecules involved when salt is present, this clearly demonstrated the role of electrostatics (Fig. 7). The larger nanostructure induced by the presence of salt enables interactions with heparin which can be optimised more effectively to give strong electrostatic binding (Table S2). These stronger interactions can form more easily for the larger nanostructure because of the larger number of available surface groups. This explains the difference between the covalent nanoscale array, and the salt-responsive self-assembled multivalent one. Not surprisingly, the overall dispersion term ($\Delta E^{eff}_{disp,tot} = \Delta E^{eff}_{vdw} + \Delta G^{eff}_{np}$, Table S2), although also favourable to binding, is lower than its electrostatic counterpart, and although increasing slightly for **C22-G1** in the presence of salt, does not contribute anywhere near as much as the electrostatic term (Fig. 7). Indeed, the increase in the dispersion term from -11.63 to -19.96 kcal/mol is much less significant on a per residue basis.

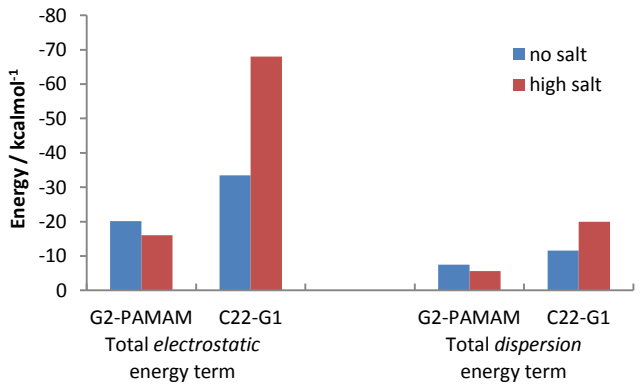

Figure 7. Deconvolution of the enthalpic term of the effective free energy of binding from multiscale modelling into effective total electrostatic and total dispersion terms – demonstrating how salt induces much stronger electrostatic binding for **C22-G1** to heparin but not for G2-PAMAM.

This combined experimental and theoretical study therefore highlights a unique and unexpected advantage of self-assembled multivalency – the dynamic, responsive and flexible stimulus-responsive nature of the SAMul array means it can significantly adapt on the nanoscale in different conditions,[21] in this case, the presence of salt, optimising multivalent binding. We believe this may be a general principle of some importance in multivalent binding and is a unique way in which self-assembled multivalent nanosystems differ from their covalent counterparts.

It should be noted that multiple micellar nanostructures will, of course, interact with each heparin chain, leading to larger hierarchical aggregates. This type of aggregation process is well-known to occur when protamine binds heparin.[22] DLS supported this viewpoint for **C22-G1**. The aggregates formed by **C22-G1** and heparin were much larger than the individual micelles or heparin chains (Table 4). Combined with the evidence from SEM and Nile Red assays, we propose that the individual micelles remain intact within these larger aggregates.

Table 4. Dynamic Light Scattering (DLS) data for **C22-G1** in the absence and presence of heparin.

	Mol Ratio	Diameter (nm)	PDI
Heparin (0.329 mg/mL)	-	8.7	0.316
C22-G1 (1.00 mg/mL)	-	9.0	0.461
C22-G1 + Heparin	0.1:1	13.0	0.276
C22-G1 + Heparin	0.5:1	68.9	0.155
C22-G1 + Heparin	1:1	too large	-

Effect of Human Serum on SAMul Heparin Binding

We next decided to probe binding in even more biologically relevant and challenging conditions – human serum. Serum is electrolytically rich and contains all of the proteins (except those involved with blood clotting), antibodies, antigens, hormones and other exogenous and endogenous species routinely present in blood. The ability of a binder to function in serum would suggest a propensity to operate in blood: the ultimate target medium for clinical application.

Table 5. Heparin Binding Data from MalB Competition Assays using 25 μM MalB and 27 μM heparin, with the heparin being delivered in 100% human serum, 10 mM Tris-HCl.

Binder	EC_{50} (μM)	CE_{50}	Dose (mg/100IU)
C22-G1	25.90 ± 1.60	0.96 ± 0.06	0.79 ± 0.05
Protamine	3.51 ± 0.12	0.79 ± 0.03	0.49 ± 0.02
G2-PAMAM	2.15 ± 0.05	0.32 ± 0.01	0.21 ± 0.01

We assayed the ability of **C22-G1**, protamine and G2-PAMAM to bind heparin delivered in 100% human serum (Table 5). This appears to somewhat disrupt the ability of **C22-G1** to displace MalB from its complex with heparin, increasing the CE_{50} value from 0.28 (Table 1) to 0.96 (Table 5). Protamine was, in relative terms, less adversely affected, with the CE_{50} value rising from 0.52 (Table 1) to only 0.79 (Table 5). Although salt enhanced the relative heparin-binding ability of **C22-G1** compared to protamine, serum therefore somewhat diminishes it. In contrast to protamine and **C22-G1**, G2-PAMAM actually decreased its CE_{50} from 0.38 to 0.32, indicating it is even better able to displace MalB in human serum. This may appear to suggest that PAMAM dendrimers are best for this application, but as demonstrated in the literature, such dendrimers are not ideal for *in vivo* use.[13,23]

There is therefore a clear difference between the covalent and self-assembled nanostructures – unlike in salt, in serum the self-assembled **C22-G1** system loses some of its apparent binding capacity relative to covalent systems. We considered this may be because the SAMul nanostructures disassemble in human serum to yield individual molecular building blocks, each of which would only have four poorly organised positive charges. Disassembly of micelles in serum is known,[24] for example, the hydrophobic units can bind to albumin and/or globulin proteins, and interact with charged surface patches on serum proteins. We probed the effect of albumin on complexes

formed between **C22-G1** and heparin using DLS (Table 6) – on exposure to albumin, the aggregates gradually (over time) became smaller, which may be explained by some destabilisation of the **C22-G1** assemblies, lowering their affinity for heparin somewhat – but the binding is clearly not completely switched off, or the aggregates completely disassembled.

Importantly, non-self-assembling analogues were completely unable to displace MalB in serum, and we therefore reasoned that **C22-G1** does not completely disassemble in human serum, and that its self-assembly is only partially compromised. In order to probe the effect of serum in more detail, we monitored the ability of **C22-G1** to displace MalB in the presence of increasing amounts of serum. We noted that on increasing serum levels from 1% to 10% there was a sequential increase in the disruption of binding. Human serum (10%) induced a similar disruption in binding to 100% (see supp info).

Table 6. Dynamic Light Scattering (DLS) data for **C22-G1** and heparin in the absence and presence of albumin (1 mg/mL),

	Mol Ratio	Diameter (nm)	PDI
C22-G1 + Heparin	0.5:1	68.9	0.155
C22-G1 + Heparin + Albumin	0.5:1	62.6	0.272
C22-G1 + Heparin + Albumin (after 30 min)	0.5:1	55.9	0.220

Although the binding of **C22-G1** to heparin in human serum is disrupted more than covalent analogues, it was still effective (CE_{50} <1.0), and given the other potential advantages of our SAMul approach,[4a] we were nonetheless encouraged to press on with further studies.

Degradation and Disassembly of C22-G1 at Biological pH

A key advantage of a SAMul approach to heparin binding is that the resulting nanostructures are potentially degradable. This can occur through (i) simple nanoparticle disassembly, or (ii) triggered bond cleavage. The design of **C22-G1** incorporates an ester linkage between the hydrophobic tail and the hydrophilic heparin-binding unit. Esters are well-known to degrade under biological conditions of pH and/or in the presence of enzymes. Both our group,[18d,25] and that of Fréchet,[26] have probed the disassembly of related dendrons and reported this as a means of achieving temporary multivalency in biological systems, and limiting biopersistence/toxicity. In this case, cleavage of the ester bond would lead to loss of the amphiphilic character of **C22-G1** and in addition to dendron breakdown, should trigger complete disassembly of the SAMul nanostructure, switching off its biological activity.

We used mass spectrometric (MS) analysis in the presence of an internal standard (Gly-Ala) to look at the loss of molecular ion. At time zero, the molecular ions associated with **C22-G1** (*m/z* = 433 $[M]^{2+}$ and 289 $[M]^{3+}$) could be seen – there was also some evidence for ester hydrolysis (alcohol, *m/z* = 408 [1+]; carboxylic acid, *m/z* = 239 $[M]^{2+}$) (see SI for full data). After 24 hours, the molecular ions for intact **C22-G1** had completely disappeared, and the peaks for ester hydrolysis were dominant, along with a peak corresponding to decarboxylation of the carboxylic acid hydrolysis product (*m/z* = 217, $[M]^{2+}$). This demonstrates that degradation of this compound is relatively facile under biologically relevant conditions of pH.

We then wanted to demonstrate that degradation would cause nanostructure disassembly. We left **C22-G2** in PBS buffer in the presence of Nile Red,[17] in order to probe whether degradation over a 24 hour timescale led to disassembly and release of encapsulated Nile Red. At time zero, the fluorescence intensity was high, as intact **C22-G1** self-assembled and encapsulated Nile Red (Fig. 8). After 24 hours, the fluorescence had dropped back close to the level observed for Nile Red in the absence of **C22-G1**. As such, we conclude that degradation of **C22-G1** leads to nanoscale disassembly.

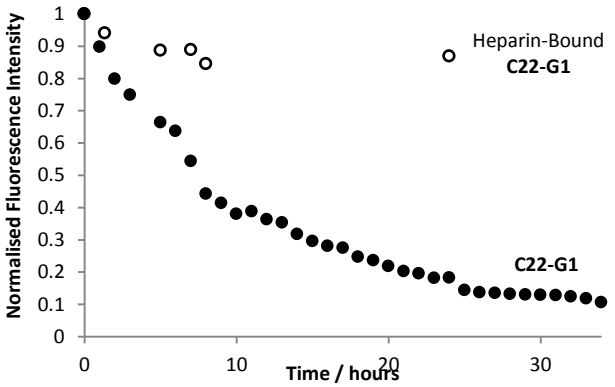

Fig. 8. Fluorescence intensity of Nile Red in PBS Buffer over 24 hours in the presence of **C22-G1** and **C22-G1** with heparin.

We repeated this Nile Red release study in the presence of heparin (Fig. 8). It should be noted that in this experiment, the **C22-G1**-heparin complexes slowly sedimented from solution owing to their large nanoscale dimensions (see DLS data presented above) – as such, the vial was gently inverted prior to each spectroscopic measurement to ensure mixing. After 24 hours, there was still a significant fluorescence intensity associated with Nile Red. This suggests that in the presence of heparin, **C22-G1** is much more resistant to degradation, and the nanoscale micelles retain their stability.

This agrees with our previous studies of related DNA-binding systems which showed that when bound to DNA, intramolecular amine catalysis of ester degradation was inhibited and the multivalent system retained both stability and DNA binding ability.[18d] As such, the degradation profile of **C22-G1** is of potential therapeutic use for heparin rescue. Excess **C22-G1** will degrade and disassemble over a relatively rapid timescale, minimising adverse effects, but **C22-G1** bound to heparin, is more stable, hopefully allowing excretion of the complex to take place prior to degradation and disassembly.

Clotting Assays Using SAMul in Human Plasma

Ultimately, the most important functional test of **C22-G1** is whether it can reverse the effect of heparin in a biomedically-relevant assay. This was probed by determining the ability of

C22-G1 to reverse heparin-induced anti-coagulation. Blood clotting (thrombogenesis) occurs in two stages:[27] (i) platelets form a cross-linked plug at the site of injury, (ii) a complex cascade of clotting factors convert soluble plasma glycoprotein fibrinogen to insoluble fibrin. This blood coagulation cascade can be simplified into two pathways: (i) the 'intrinsic pathway' originating from surface contact trauma, (ii) the 'extrinsic' pathway originating from tissue damage. The intrinsic pathway plays a minor role in overall clotting and can be monitored by measuring an activated partial thromboplastin time (aPTT assay). In the extrinsic pathway, there are relatively few steps from initial trauma to the production of Factor Xa which is required in large amounts, and this is therefore the dominant route in the overall coagulation cascade – it is monitored by measuring prothrombin clotting time (PT assay).

Table 7. Heparin Binding Data from aPTT and PT clotting assays in human plasma.

	Clotting Time (s)	
	aPTT Assay[a]	PT assay[b]
Plasma Only	35.7 ± 0.7	12.8 ± 0.8
+ Heparin	None	None
+ C22 G1	81.8 ± 4.6	13.1 ± 0.4

a: aPTT assay performed with 2.5 units of heparin dose and C22-G1 applied at 0.79 mg/100IU. b: PT assay performed with 5 units of heparin dosed and C22-G1 applied at 0.79 mg/100 IU.

We monitored the ability of **C22-G1** to reverse the effect of heparin using aPTT (intrinsic) and PT (extrinsic) assays (Table 7). In the absence of heparin, the plasma clotted in 35.7 s (aPTT assay) and 12.8 s (PT assay). On the addition of heparin, clotting no longer occurred, as heparin exerted its anti-coagulant effect. We then added **C22-G1** at an appropriate dose. In both assays, **C22-G1** induced clotting – demonstrating it is capable of functional heparin reversal. In the aPTT assay, the clotting time was somewhat elevated at 81.8 s, but in the PT assay, the clotting time was very similar to native plasma, at 13.1 s. These experiments demonstrate that even though our binding studies in 100% human serum indicated some decrease in heparin affinity, these self-assembled multivalent systems are active in plasma. Clearly, if we can further stabilise the SAMul nanostructures, we may be able to further enhance heparin binding and clotting times, particularly in the aPTT assay. Nonetheless, it is clear that with appropriate optimisation of structure, dosage and delivery mode, SAMul systems such as **C22-G1** are potentially very promising therapeutic agents for heparin rescue.

Conclusions

In conclusion, **C22-G1** is a heparin binder in which self-assembly into nanoscale structures plays a key role in multiplying up the ligand array for multivalent heparin binding. The dynamic and responsive nature of self-assembly means that the addition of salt changes the dimensions of the self-assembled nanostructure and increases heparin binding affinity relative to fixed covalent nanostructures – a unique feature of the SAMul approach. The presence of serum adversely affects heparin affinity relative to covalent nanostructures, which we assign to partial destabilisation of the self-assemblies under these conditions. Degradation and disassembly take place as a result of ester hydrolysis, leading to loss of SAMul binding over a 24 hour timescale, but once bound to heparin, the nanostructure is more stable – a clinically useful profile. Clotting assays in human plasma demonstrate that **C22-G1** acts as a functional heparin reversal agent, and we therefore suggest that this general approach has clinical potential. Further optimisation of these SAMul systems and extended structure-activity relationship studies are currently underway in order to (i) better understand heparin binding in fundamental terms, and (ii) further stabilise the self-assemblies prior to clinical application in highly competitive human blood.

Acknowledgements

SMB and DKS thank BBSRC and University of York for funding (DTA award) and COST Network TD0802 (Dendrimers in Biomedicine) for supporting networking within this project. We acknowledge support from the University of York Centre of Excellence in Mass Spectrometry created thanks to a major capital investment through Science City York, supported by Yorkshire Forward with funds from the Northern Way Initiative. Access to CINECA and supercomputing facility was granted to SP and PP through the sponsored HPC Italian Supercomputing Resource Allocation (ISCRA) projects MONALISA, NANO4HEALTH and SEA.

Notes and references

[a] Department of Chemistry, University of York, Heslington, York, YO10 5DD, UK. Fax: +44 (0)1904 324516. E-mail: david.smith@york.ac.uk..

[b] Simulation Engineering (MOSE) Laboratory, Department of Engineering and Architecture (DEA), University of Trieste, 34127, Trieste, Italy.

[c] National Interuniversity Consortium for Material Science and Technology (INSTM), Research Unit MOSE-DEA, University of Trieste, 34127 Trieste, Italy.

[d] Institut for Chemie and Biochemie, Freie Universität Berlin, Takustrasse 3, D-14195 Berlin, Germany

[e] Institute of Integrative Biology, Biosciences Building, University of Liverpool, Crown Street, Liverpool L69 7ZB, UK.

† The manuscript was written through contributions of all authors. All authors have given approval to the final version of the manuscript.

‡ These authors contributed equally to this work.

Electronic Supplementary Information (ESI) available: Full experimental methods for all assays, titration curves, simulation details. See DOI: 10.1039/b000000x/

1. (a) R. Duncan and R. Gaspar, *Mol. Pharm.* 2011, **8**, 2101-2141. (b) B. Y. S. Kim, J. T. Rutka and W. C. W. Chan, *New Engl. J. Med.* 2010, **363**, 2434-2443.
2. (a) D. A. Uhlenheuer, K. Petkau and L Brunsveld, *Chem. Soc. Rev.* 2010, **39**, 2817-2826. (b) D. K. Smith, *J. Chem. Educ.* 2005, **82**, 393-400.
3. (a) M. Mammen, S. K. Choi and G. M. Whitesides, *Angew. Chem. Int. Ed.* 1998, **37**, 2755-2794. (b) A. Mulder, J. Huskens and D. N.

Reinhoudt, *Org. Biomol. Chem.* 2004, **2**, 3409-3424. (c) C. Fasting, C. A. Schalley, M. Weber, O. Seitz, S. Hecht, B. Koksch, J. Dernedde, C, Graf, E. W. Knapp and R. Haag, *Angew. Chem. Int. Ed.* 2012, **51**, 10472-10498.

4. (a) A. Barnard and D. K. Smith, *Angew. Chem. Int. Ed.* 2012, **51**, 6572-6581. (b) K. Petkau-Milroy and L. Brunsveld, *Org. Biomol. Chem.* 2013, **11**, 219-232. (c) P. M. Levine, T. P. Carberry, J. M. Holub and K. Kirshenbaum, *Med. Chem. Commun.* 2013, **4**, 493-509.
5. (a) J. E. Kingerywood, K. W. Williams, G. B. Sigal and G. M. Whitesides, *J. Am. Chem. Soc.* 1992, **114**, 7303-7305. (b) J. D. Hartgerink, E. Beniash and S. I. Stupp, *Science* 2001, **294**, 1684-1688. (c) G. Thoma, A. G. Katopodis, N. Voelcker, R. O. Duthaler and M. B. Streiff, *Angew. Chem. Int. Ed.* 2002, **41**, 3195-3198. (d) G. A. Silva, C. Czeisler, K. L. Niece, E. Beniash, D. A. Harrington, J. A. Kessler and S. I. Stupp, *Science* 2004, **303**, 1352-1355. (e) M. K. Muller and L. Brunsveld, *Angew. Chem. Int. Ed.* 2009, **48**, 2921-2924. (f) D. J. Welsh and D. K. Smith, *Org. Biomol. Chem.* 2011, **9**, 4795-4801. (g) D. J. Welsh, P. Posocco, S. Pricl and D. K. Smith, *Org. Biomol. Chem.* 2013, **11**, 3177-3186.
6. S. M. Bromfield, E. Wilde and D. K. Smith, *Chem. Soc. Rev.* 2013, **42**, 9184-9195.
7. (a) R. Barbucci, A. Magnani, S. Lamponi, A. Albanese, *Polym. Adv. Technol.* 1996, **7**, 675-685. (b) D. L. Rabenstein, *Nat. Prod. Rep.* 2002, **19**, 312-331. (c) S. Middeldorp, *Thromb. Res.* 2008, **122**, 753-762.
8. R. Balhorn, *Genome Biol*. 2007, **8**, 227.
9. (a) M. Nybo and J. S. Madsen, *Basic Clin. Pharmacol.* 2008, **103**, 192-196. (b) Y.-Q. Chu, L.-J. Cai, D.-C. Jiang, D. Jia, S.-Y. Yan and Y.-Q. Wang, *Clin. Ther.* 2010, **32**, 1729-1732.
10. C. Hermans and D. Claeys, *Curr. Med. Res. Opinion* 2006, **22**, 471-481.
11. (a) M. Kikura, M. K. Lee and J. H. Levy, *Anesth. Analg*. 1996, **83**, 223-227. (b) T. W. Wakefield, P. C. Andrews, S. K. Wrobleski, A. M. Kadell, A. Fazzalari, B. J. Nichol, T. Van der Kooi and J. C. Stanley, *J. Surgical Res.* 1994, **56**, 586-593. (c) R. E. McAllister, *Circulation* 2010, **122**, A17322. (d) J. Kuziej, E. Litinas, D. A. Hoppensteadt, D. Liu, J. M. Walenga, J. Fareed, W. Jeske, *Clin. Appl. Thromb. Hemost.* 2010, **16**, 377-386. (e) F. Cunsolo, G. M. L. Consoli, C. Geraci and T. Mecca, *Abiotic Heparin Antagonists* WO/2005/028422. (f) T. Mecca, G. M. L. Consoli, C. Geraci, R. La Spina and F. Cunsolo, *Org. Biomol. Chem.* 2006, **4**, 3763-3768. (g) T. Mecca and F. Cunsolo, *Poly. Adv. Tech*. 2010, **21**, 752-757. (h) S. Choi, D. J. Clements, V. Pophristic, I. Ivanov, S. Vemparala, J. S. Bennett, M. L. Klein, J. D. Winkler and W. F. DeGrado, *Angew. Chem. Int. Ed.* **2005**, *44*, 6685-6689. (i) M. Schuksz, M. M. Fuster, J. R. Brown, B. E. Crawford, D. P. Ditto, R. Lawrence, C. A. Glass, L. Wang, Y. Tor and J. D. Esko, *Proc. Natl. Acad. Sci. USA* 2008, **105**, 13075-13080.
12. (a) W. A. Weiss, J. S. Gilman, A. J. Catenacci and A. E. Osterberg, *J. Am. Med. Assoc.* 1958, **166**, 603-607. (b) C. W. Lillehei, L. P. Stems, D. M. Long and D. Lepley, *Ann. Surg.* 1960, **151**, 11-16. (c) G. Montalescot, W. M. Zapol, A. Carvalho, D. R. Robinson, A. Torres, E. Lowenstein, *Circulation* 1990, **82**, 1754-1764. (d) K. Kaminski, M. Plonka, J. Ciejka, K. Szczubialka, M. Nowakowska, B. Lorkowska, T. Korbut and R. Lach, *J. Med. Chem.* 2011, **54**, 6586-6596. (e) B. Kalanska, E. Sokolowska, K. Kaminski, K. Szczubialka, K. Kramkowski, A. Mogielnicki, M. Nowakowska and W. Buczko, *Eur. J. Pharmacol.* 2012, **686**, 81-89. (f) S. Bai, C. Thomas and F. Ahsan, *J. Pharm. Sci.,* 2007, **96**, 2090-2106. (g) X. Feng, Y. Cheng, K. Yang, J. Zhang, Q. Wu, T. Xu, *J. Phys. Chem. B*, 2010, **114**, 11017-11026. (h) S. Bai and F. Ahsan, *Pharm. Res*. 2009, **26**, 539-545.
13. R. Duncan and L. Izzo, *Adv. Drug Deliv. Rev.* 2005, **57**, 2215-2237.
14. A. C. Rodrigo, A. Barnard, J. Cooper and D. K. Smith, *Angew. Chem. Int. Ed.* 2011, **50**, 4675-4679.
15 S. M. Bromfield, A. Barnard, P. Posocco, M. Fermeglia, S. Pricl and D. K. Smith, *J. Am. Chem. Soc.* 2013, **135**, 2911-2914
16. S. M. Bromfield, P. Posocco, M. Fermeglia, S. Pricl, J. Rodríguez-López and D. K. Smith, *Chem. Commun.* 2013, **49**, 4830-4832.
17. M. C. A. Stuart, J. C. van de Pas and J. B. F. N. Engberts, *J. Phys. Org. Chem.* 2005, **18**, 929-934.
18. (a) S. P. Jones, N. P. Gabrielson, D. W. Pack and D. K. Smith, *Chem. Commun.* 2008, 4700-4702. (b) P. Posocco, S. Pricl, S. Jones, A. Barnard and D. K. Smith, *Chem. Sci.* 2010, **1**, 393-404. (c) S. P. Jones, N. P. Gabrielson, C.-H. Wong, H.-F. Chow, D. W. Pack, M. Fermeglia, S. Pricl and D. K. Smith, *Mol. Pharm.* 2011, **8**, 416-429. (d) A. Barnard, P. Posocco, S. Pricl, M. Calderon, R. Haag, M. E. Hwang, V. W. T. Shum, D. W. Pack and D. K. Smith, *J. Am. Chem. Soc.* 2011, **133**, 20288-20300.
19. P. Posocco, E. Laurini, V. Dal Col, D. Marson, L. Peng, D. K. Smith, B. Klajnert, M. Bryszewska, A.-M. Caminade, J. P. Majoral, M. Fermeglia, K. Karatasos and S. Pricl, in *Biomedical Applications of Dendrimers*, Ed. B. Klajnert, L. Peng and V. Cena, RSC, Cambridge, pp 148-166, 2013.
20. (a) J.-M. Chen, Y.-M. Su and Y. Mou, *J. Phys. Chem.* 1986, **90**, 2418-2421. (b) V. K. Aswal and P. S. Goyal, *Chem. Phys. Lett.* 2002, **364**, 44-50.
21. J. Zhuang, M. Gordon, J. Ventura, L. Li and S. Thayumanavan, *Chem. Soc. Rev.* 2013, **42**, 7421-7435.
22. (a) P. Rossman, K. Matousovic, V. Horacek, *Virchows Archiv B: Cell Pathol incl Mol. Pathol.* 1982, **40**, 81-98. (b) G. Stehle, A. Wunder, H. Sinn, H. H. Schrenk, E. A. Friedrich, C. E. Dempfle, W. Maierborst and D. L. Heene, *J. Surgical Res.* 1995, **58**, 197-204. (c) J. Maurer, S. Haselbach, O. Klein, D. Baykut, V. Vogel and W. Mantele, *J. Am. Chem. Soc.* 2011, **133**, 1134-1140.
23. N. Malik, R. Wiwattanapatapee, R. Klopsch, K. Lorenz, H. Frey, J. W. Weener, E. W. Meijer, W. Paulus and R. Duncan, *J. Controlled Release* 2000, **65**, 133-148.
24. (a) S. Kim, Y. Z. Shi, J. Y. Kim, K. Park, J. X. Cheng, *Expert Opin. Drug Deliv.* 2010, **7**, 49-62. (b) T. Miller, A. Hill, S. Uezguen, M. Weigandt and A. Goepferich, *Biomacromolecules* 2012, **13**, 1707-1718. (c) J. Lu, S. C. Owen and M. S. Shoichet, *Macromolecules* 2011, **44**, 6002-6008.
25. D. J. Welsh, S. P. Jones and D. K. Smith, *Angew. Chem. Int. Ed.* 2009, **48**, 4047-4051
26. (a) E. R. Gillies and J. M. J. Fréchet, *J. Am. Chem. Soc.* 2002, **124**, 14137-14146. (b) E. R. Gillies, E. Dy, J. M. J. Fréchet and F. C. Szoka, *Mol. Pharm.* 2005, **2**, 129-138. (c) C. C. Lee, E. R. Gillies, M. E. Fox, S. J. Guillaudeu, J. M. J. Fréchet, E. E. Dy and F. C. Szoka, *Proc. Natl. Acad. Sci. USA* 2006, **103**, 16649-16654.
27. S. M. Bates and J. I. Weitz, *Circulation* 2005, **112**, e53-e60.

Graphical Abstract:

Dynamic and responsive self-assembled multivalent ligand arrays yield functional heparin reversal in highly competitive media such as human plasma.